Quaternary Geochronology 74 (2023) 101415

Contents lists available at ScienceDirect

Quaternary Geochronology

journal homepage: www.elsevier.com/locate/quageo

Accurate chronological construction for two young stalagmites from the tropical South Pacific

Mohammadali Faraji [a,*], Silvia Frisia [a], Quan Hua [b], Andrea Borsato [a], Monika Markowska [c]

[a] School of Environmental and Life Sciences, The University of Newcastle, NSW, 2308, Australia
[b] Australian Nuclear Science and Technology Organisation, Locked Bag 2001, Kirrawee DC, NSW, 2232, Australia
[c] Climate Geochemistry Department, Max Planck Institute for Chemistry, 55128, Mainz, Germany

ARTICLE INFO

Keywords:
Radiocarbon
Chronological construction
Southern Cook Islands
Speleothems
Tropical South Pacific

ABSTRACT

Modern to Holocene tropical Pacific stalagmites are commonly difficult to date with the U-series, the most commonly used dating method for speleothems. When U-series does not provide robust age models, due to multiple sources of ^{230}Th or little U, radiocarbon is, potentially, the best alternative. The ^{14}C content of two stalagmites (Pu17 and Nu16) collected from Pouatea and Nurau caves in the Cook Island Archipelago of the South Pacific were measured to obtain accurate chronology for their most modern parts. The bomb-pulse soil continuum modelling indicates that bomb radiocarbon in Pu17 onsets in 1956 and reaches its maximum in 1966 CE, suggesting a fast transfer of atmospheric carbon to the stalagmite of <1 year. The modelling for Pu17 suggests a 20% contribution from C_1 - an instantaneous carbon source, which renders possible an immediate transfer of atmospheric signal into the cave. Nu16 shows a slower transfer of atmospheric carbon to the stalagmite than Pu17, with bomb radiocarbon onsetting in 1957 CE and peaking in 1972 CE. The less negative δ^{13}C values in Nu16 than Pu17, and also the modelling corroborated this, which points out no contribution from the instantaneous carbon source. The radiocarbon age models and laminae counting age models were then spliced to achieve a single master chronology for the top part of each stalagmite. This study is an example of ^{14}C age modelling combined with visible physical and chemical laminae counting and how it can improve the accuracy and precision of dating for otherwise hard-to-date tropical Pacific speleothems. Such accurate and precise age models pave the way to obtain sub-annually resolved paleoclimate records by further improving the calibration of climate proxy data with the current and instrumental weather parameters.

1. Introduction

In the last couple of decades, speleothems have been used to develop terrestrial paleoclimate reconstructions on a wide range of temporal resolutions from seasonal to millennial scales (Fairchild and Baker, 2012). These records are now available for different climate settings (e.g. Bar-Matthews et al., 1999; Li et al., 2005; Vansteenberge et al., 2020; Wang et al., 2019), but scarce for the South Pacific islands. Additionally, the instrumental records in this region are typically short and incomplete, providing only a snap-shot of the range of regional natural climate variability. The South Pacific islanders are highly vulnerable to the effects of both climate variability (Cai et al., 2015) and climate change (Held and Soden, 2006; Xie et al., 2010). However, as Widlansky et al. (2012) highlighted, there is significant uncertainty in how the South Pacific Convergence Zone (SPCZ), the largest rainband in the Southern Hemisphere, will respond in the future under a changing climate. Therefore, there is sufficient justification for developing robust, accurately dated paleoclimate reconstructions from stalagmites, given that in this region, water for agriculture is almost entirely supplied by rainfall rather than by irrigation systems (Barnett, 2011).

One of the strengths of speleothems as a paleoclimatic archive is, arguably, their capability to be accurately and precisely dated via radiometric methods (Dorale et al., 2004; Harmon et al., 1977; Hellstrom, 2006; Richards et al., 1998; Scholz and Hoffmann, 2008; Zhao et al., 2003). The U-series disequilibrium method is the most commonly used dating method for speleothems (Hellstrom, 2003). In the case that U–series dating cannot be applied, for example, because of multiple sources of ^{230}Th (Hua et al., 2012), robust relative chronologies can be acquired via counting annual visible chemical and physical laminae (Baker et al., 2021) on two-dimensional maps (Faraji et al., 2021; Oriani

* Corresponding author.
E-mail address: mohammadali.faraji@uon.edu.au (M. Faraji).

https://doi.org/10.1016/j.quageo.2022.101415
Received 20 February 2022; Received in revised form 14 November 2022; Accepted 20 November 2022
Available online 23 November 2022

et al., 2022). This approach may also entail considerable uncertainties, particularly in the youngest, modern parts of the speleothem due to fabric complexity maps (Faraji et al., 2021). An alternative method for obtaining accurate age models and further constraining the age of modern speleothems (1950 CE – present) is using the radiocarbon [^{14}C] “bomb-pulse” method (e.g. Genty and Massault, 1999; Hodge et al., 2011; Hua et al., 2012; Markowska et al., 2019; Mattey et al., 2008; Noronha et al., 2015; Scroxton et al., 2021). Calibrated radiocarbon ages can also be used as an age constraint up to ~50 ka. However, its use in speleothems is complicated by the contribution of ‘radioactively dead’ carbon, known as Dead Carbon Proportion (DCP), derived from ^{14}C-depleted material from bedrock and aged soil organic matter. Consequently, when comparing the radiocarbon ages of speleothems to the ages obtained by the U–Th method, they commonly show older ages (Beck et al., 2001; Goslar et al., 2000). A thorough understanding of DCP variations in a speleothem then can pave the way to generate a reliable radiocarbon chronology and also gain insight into the variability of water-rock interactions through time (Bajo et al., 2017; Griffiths et al., 2012).

We studied two stalagmites (Pu17 from Pouatea cave and Nu16 from Nurau cave) retrieved from Atiu Island, in the South Pacific to obtain accurate and precise chronologies, which is fundamental for robust paleoclimate reconstructions. Similar to other speleothems from Pacific Island caves, which are cut in reef limestone, speleothems in Atiu are expected to provide an excellent opportunity for radiocarbon dating. That is because the rock burden above caves is 2–8 m, characterized by high porosity resulting from incomplete diagenesis of a relatively young reef. This shallow cave system, coupled with a limited and patchy soil

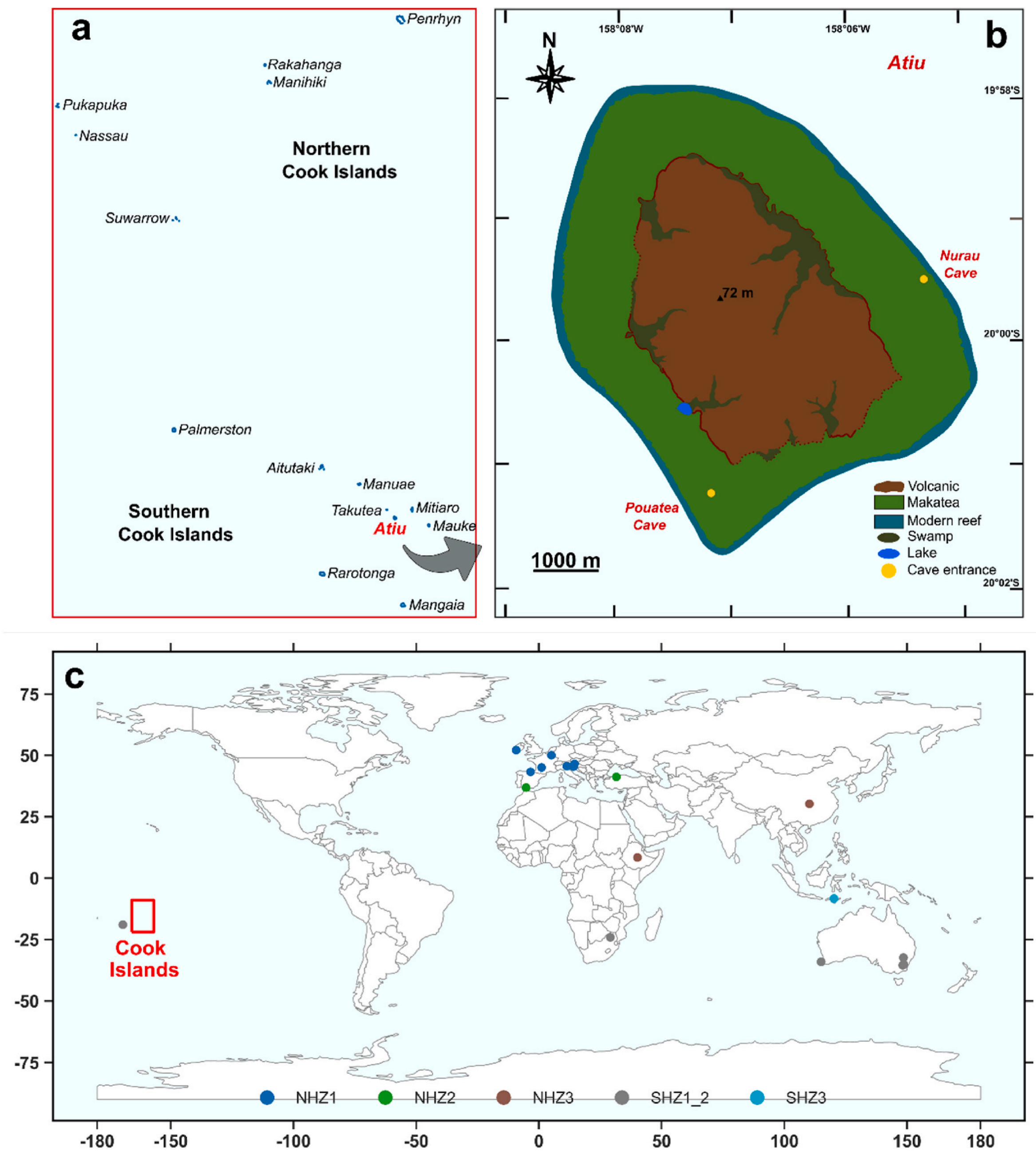

Fig. 1. a, the Northern and Southern groups of the Cook Islands (redrawn from Australian Bureau of Meteorology and CSIRO (2011)). b, Geomorphological map of Atiu Island (redrawn from Stoddart et al. (1990)) with the location of Pouatea and Nurau caves. c, location of Cook Islands and the bomb-pulse radiocarbon chronologies in the literature that was referred to in this study, the majority of which are from Northern Hemisphere Zone 1 (NHZ1). The stalagmite radiocarbon chronologies plotted in “c” are grouped according to the atmospheric ^{14}C zones defined in Hua et al. (2021).

cover, ensures rapid surface climate conditions transmission into the cave. Except for some small pockets of red clay soil filling the bottom of joint-controlled karst of colluvial origin (Stoddart et al., 1990), the surface above the cave is bare karst. Rapid transmission of rain signal into the cave reduces the interaction between rainwater and bedrock, thus, minimizing the contribution of bedrock-derived dead carbon, which is crucial for constructing reliable radiocarbon age-depth models.

In this study, we develop a chronology for modern portions of the two stalagmites from Atiu Island by using ^{14}C and the *bomb pulse soil continuum* method from Markowska et al. (2019). We then compare different chronologies available for Pu17 and Nu16, including laminae counting and radiocarbon age models, and discuss how they are combined to obtain accurate and precise chronologies, which pave the way towards reconstructing hydroclimate variability from speleothems that are difficult to date in their modern parts.

2. Sample and site description

The stalagmites selected for this study were retrieved from Atiu Island (7.25 km N–S and 6.3 km E-W), the third-largest island in the Southern Cook Islands, located in latitude 20°S and longitude 158°10′W in the South Pacific (Fig. 1a and b). Atiu, as described by Stoddart et al. (1990), is a highly eroded volcanic island surrounded by a rim of elevated Cenozoic reefal limestone (i.e., the makatea - the Polynesian word for “white stone” referring to the reef limestone (Kirch, 2000)). The volcanic plateau of Atiu reaches a maximum height of ≈72 m above sea level (asl), mainly covered with limonitic-nodule-bearing red clay. Based on foraminifera fossils, a Plio-Pleistocene age was attributed to the uplifted reefal limestone that once rimmed the volcanic island (Marshall, 1930).

The vegetation above both Nurau and Pouatea caves is thick, and soil cover is limited to patchy areas where it has concentrated in dissolution pits and trenches. Alfisols, Mollisols and Inceptisols are the main types of soils covering the island (Bruce, 1983). However, most of the karstified makatea is barren limestone, where tree roots find their way underground through dissolution cracks and voids in the absence of soil. The indigenous forest association above the caves consists of native *Elaeocarpus tonganus* and *Hernandia moerenhoutiana*. Alien species, typically coconut palms, mark human impact (Holland and Olson, 1989). Although a large number of weedy plants have become naturalized in the central volcanic interiors of Atiu, alien species have generally not been able to spread into the makatea.

2.1. Pouatea cave and stalagmite Pu17

Stalagmite Pu17 (Fig. 2) was actively growing when removed in March 2019 at a depth of ca. 7 m beneath the surface within a gallery leading to the cave’s southern dead-end (Faraji et al., 2021). Pu17 was fed by a relatively slow and constant drip (1 drop every 15 min), which resulted in its candle-shaped morphology (cf. Miorandi et al., 2010). There were strong indications that the stalagmites were actively growing, evidenced by the analysis of several dripwater in the cave indicating a pH of ≈8 and the measured dripwater Saturation Index for calcite (SIcc) between 0.9 and 1. Additionally, we observed calcite forming in situ on watch glasses placed under both relatively fast (1 drop per 11 s) and slow (1 drop per 50 s) drips. Stalagmite Pu17 is 53 mm long

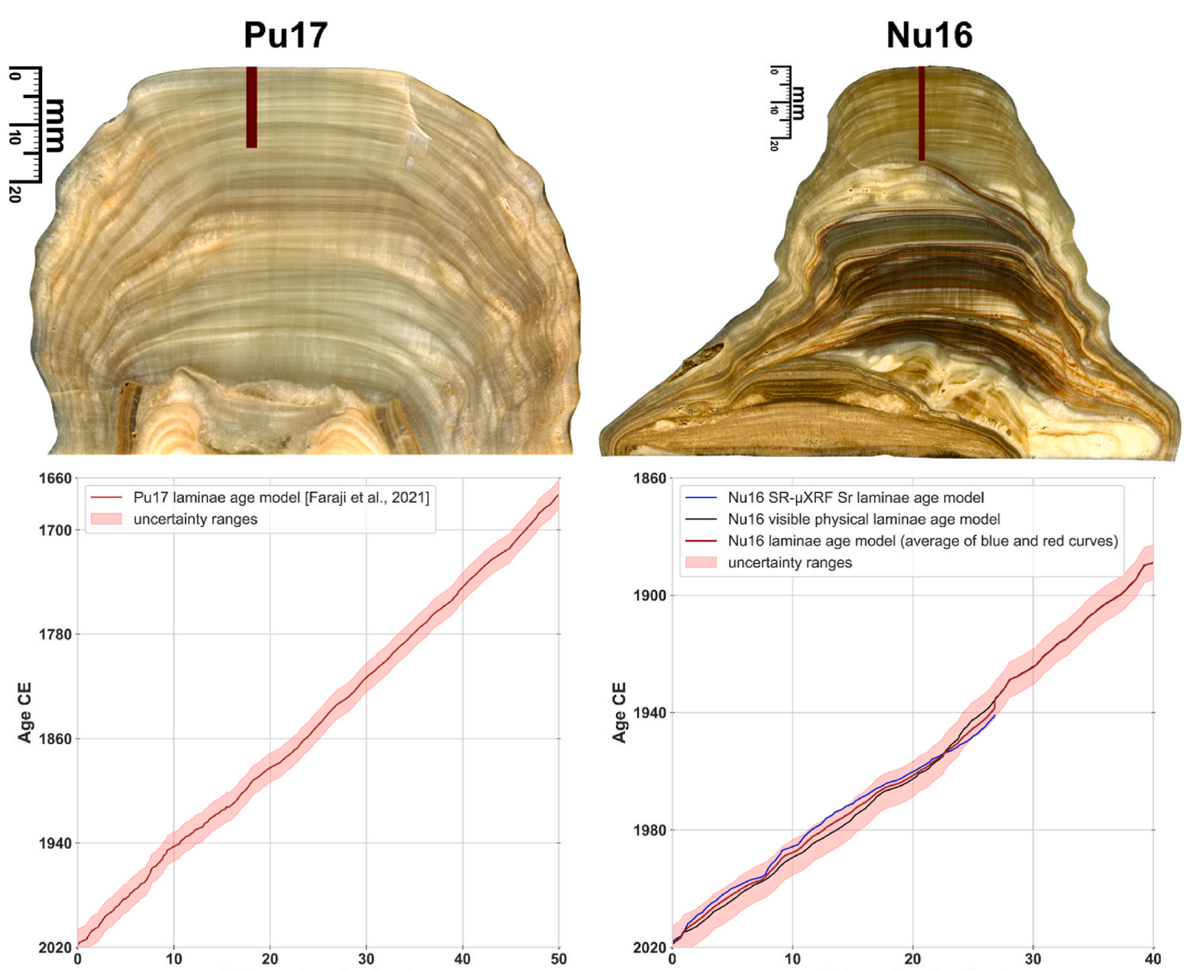

Fig. 2. Stalagmites Pu17 and Nu16, and their laminae counting chronologies. The red bars on the speleothem scans (top panels) show the portions analyzed for ^{14}C.

and grew over a stalagmite stump, likely broken by humans, which highlights the importance of speleothems as a ceremonial building material, according to Atiuan lore (Trotter and Duff, 1974). The stalagmite provides an opportunity to unravel the history of Polynesian land use as well as climate variability.

Pouatea cave (20°01′12″S, 158°07′10″W), located on the south-western side of Atiu island, is a cave network with several intersecting passages and side galleries with a total surveyed length of 1200 m. The cave's main entrance is a vertical shaft with a drop of about 4 m that opens 23 m asl at 525 m from the shoreline. There are five other entrances (skylights) with diameters ranging from 3 to 10 m formed due to cave roof collapse. The rock overburden is 4–8 m thick, characterized by high porosity, likely due to a relatively young reef's incomplete diagenesis. The porous epikarst ensures rapid transmission of water through the vadose zone, further accelerated by the thin and patchy soil cover.

2.2. Nurau cave and stalagmite Nu16

Stalagmite Nu16 (Fig. 2) was retrieved from Nurau Cave in October 2018 at a depth of ca. 8 m beneath the surface from a dead-end chamber. Nu16 is a 100 mm long candle-shaped stalagmite. It was actively growing over a flowstone at the time of removal and was fed by a honey-coloured soda-straw stalactite. The drip rate varied from 1 drop/318 s in the relatively dry season (measured in October 2018) to 1 drop/48 s in the wet season (measured in March 2019). Nu16 shows clear laminations throughout its growth, permitting a chronology to be constructed by counting the visible laminae.

Nurau cave (19°59′37″S, 158°05′18″W) is located on the eastern side of Atiu island. The cave entrance, which is a narrow passage at the bottom of a skylight, is 250 m from the shoreline and ca. 19 m asl. Nurau was surveyed in 2018 for a total length of 500 m. Similar to other caves in Atiu, Nurau is a solution-maze cave system containing several intersecting passages and side galleries. The rock burden above the cave varies between 2 and 8 m and consists of porous reefal limestone, characterized by evidence of old palaeokarst in the form of dissolution cavities filled by calcite cement crusts.

3. Methods

Prior to constructing radiocarbon chronologies for Pu17 and Nu16, other techniques such as U–Th dating coupled with counting visible physical and chemical laminae were applied that led to reasonably accurate age models. This was then followed by radiocarbon measurements and building ^{14}C age models using the soil carbon continuum modelling (Markowska et al., 2019) that enhanced the accuracy of initial laminae and U–Th models. The final chronology for each stalagmite was constructed by splicing the laminae counting and radiocarbon age models.

3.1. Laminae counting chronology

Using high-frequency variations in visible growth laminae properties (Baker et al., 2015; Tan et al., 2006) or the cyclicity of their geochemical properties, such as trace element concentration (Ban et al., 2018; Borsato et al., 2007; Jamieson et al., 2015; Johnson et al., 2006; Nagra et al., 2017; Orland et al., 2014; Treble et al., 2003; Wang et al., 2019), or C and O isotope ratios (Mattey et al., 2008; Treble et al., 2005) can assist in subjugating the limitations of speleothem U–Th dating, and acquiring precise relative age models. Faraji et al. (2021) reconstructed an age-depth model for Pu17 via integrating, in a multivariate analysis, high resolution (6 μm) variations in trace elements analyzed by LA-ICP-MS, with optically visible growth bands and two-dimensional Sr-concentration laminae as identified through synchrotron-radiation-based micro XRF (SR-μXRF) mapping. By tying the U–Th ages to the lamina chronology, Faraji et al. (2021) reconstructed the initial $^{230}Th/^{232}Th$ for each U–Th sample analyzed. This combined approach resulted in an age model with only 4% uncertainty, considerably improving upon the ca. 50% uncertainty in the U–Th ages. Nu16, on the other hand, yielded unreliable U/Th dates with age inversions, which could not be useful for age model building. However, a laminae counting chronology was obtained for Nu16 via coupling SR-μXRF two-dimensional Sr-concentration laminae with optical imaging of annual growth laminae. SR-μXRF microscopy that was used for building laminae counting chronology was performed on polished stalagmite samples at the XFM beamline at the Australian Synchrotron (Paterson et al., 2011) equipped with a Maia 384 detector array mounted 10 mm away from the sample target. The beam spot size was 1.5 μm, and the monochromatic incident energy was set at 18.5 keV. The XFM spectral data were analyzed using the GeoPIXE software suite, quantified by using single element Mn, Fe and Pt foils (Micromatter, Canada) and corrected by using a Ca matrix factor (Borsato et al., 2021; Fisher et al., 2015; Ryan et al., 2010).

However, accurate dating of the topmost parts of the two stalagmites remains disputable. That is because the very recent laminations are not evident, and fabrics and growth patterns are complicated (Frisia et al., 2022), likely due to the simultaneous dissolution and precipitation of calcium carbonate. Therefore, it is reasonable to examine radiocarbon as a potential dating method to build accurate chronologies for the young modern parts of the Atiuan stalagmites.

3.2. Radiocarbon analysis

Aliquots of 8–10 mg of carbonate powders were obtained from the two stalagmites using a MicroMill 2002 Desktop Milling Machine equipped with tungsten carbide dental drills with a drill bit diameter of 1 mm, and micromilling continuously at 300 μm along the central growth axis of the stalagmite. Based on the constructed lamina-based chronologies, 18 samples from the top 13 mm of Pu17 and 24 samples from the top 28 mm of Nu16 were then selected for AMS (accelerator mass spectrometry) ^{14}C analysis. In order to minimize modern atmospheric CO_2 contamination, the sampling was carried out one day before the analysis. Powdered samples were then dissolved in ~2 ml of 85% H_3PO_4. Fast carbonate dissolution and complete conversion to CO_2 were ensured by heating the sample vials on a hot block at 90 °C for 1 h. The evolved CO_2 was then converted to graphite using H_2 over Fe catalyst (Hua et al., 2001). AMS measurements were carried out using the VEGA accelerator at ANSTO (Fink et al., 2004) with a typical 1σ uncertainty of 0.25–0.3%. Results showing the ^{14}C content of the stalagmite samples were reported as percent modern carbon (pMC; Stuiver and Polach, 1977), after correction for machine background, procedural blank, and isotopic fractionation using measured $\delta^{13}C$.

3.3. Radiocarbon age-depth modelling

We employed the ^{14}C bomb-pulse method to date the modern part of the Atiu's speleothems. Building reliable radiocarbon chronologies for speleothems using this method, which exploits the global anthropogenic increase in atmospheric ^{14}C resulting from nuclear testing in the 1950s and 1960s CE, is not uncommon (e.g. Genty and Massault, 1999; Hodge et al., 2011; Hua et al., 2012; Markowska et al., 2019; Mattey et al., 2008; Noronha et al., 2015). The rising of the atmospheric ^{14}C concentrations is around 1955 CE (Hua et al., 2013, 2021), reaching its peak in the Northern Hemisphere (NH) in 1963 CE and the Southern Hemisphere (SH) in 1965 CE. The incorporation of the elevated atmospheric ^{14}C into a speleothem provides a means to determine its bomb-pulse profile. This profile was established by using two main anchor points: 1) the point where ^{14}C concentrations begin to rise, and 2) the date that the speleothem was retrieved from the cave (for active speleothems). However, ^{14}C transferred from the atmosphere to a speleothem is typically damped and lagged due to the incorporation of C from the soil organic matter above the cave, which is site-specific and has variable residence times. It is, therefore, crucial to have a thorough understanding of carbon dynamics in the soil zone. Several studies have modelled the age spectrum of soil organic matter to better understand unsaturated zone carbon dynamics (e.g. Carlson et al., 2019; Fohlmeister et al., 2011; Griffiths et al., 2012; Hodge et al., 2011; Noronha et al., 2015). Such models assume that soil gas carbon arises from three different reservoirs with fast, medium and slow turnover times. The ^{14}C content recorded in a speleothem is, thus, dictated by the relative C fraction in those reservoirs. These studies employ a wide variety of prescribed C pool ages ranging between 1 and 10,000 years to simulate the decomposition of organic C based on the humification model. One potential limitation of these models is averaged or prescribed turnover time of C pools. Markowska et al. (2019) put forward another approach that considers the decay of C as a continuum. It uses a four-reservoir model and considers $^{14}CO_2$ more broadly in terms of vadose zone (root and microbial respiration) contributions. Markowska et al. (2019)'s approach defines C pools as C_1 reservoir (turnover <1 year), bioavailable C_2 reservoir (1–5 years), intermediate, chemically or physically protected C_3 reservoir (1–40 years) and a chemically or physically protected (nonbioavailable) C_4 reservoir (1–1000 years). ^{14}C in this model is represented by an array of Weibull distributions, assuming different contributions from each reservoir. The most appropriate distribution is then determined using a solver function (Markowska et al., 2019), based on the best fit to the speleothem ^{14}C bomb-pulse profile, after accounting for a dead carbon proportion (DCP). The DCP, which is used to account for the contribution of old carbon (from soil and/or limestone bedrock), was calculated as $DCP = \left[1-\left(\frac{^{14}C_{meas.}}{^{14}C_{atm.}}\right)\right] \times 100\%$ (from Genty and Massault, 1999), where $^{14}C_{meas.}$ is the measured ^{14}C content in a speleothem and $^{14}C_{atm.}$ is the ^{14}C content of the coeval atmosphere. We followed this approach to model the soil continuum for Atiu caves and build robust radiocarbon chronologies for Pu17 and Nu16.

3.4. Construction of final chronologies

Final age models for Pu17 and Nu16 were constructed by splicing the radiocarbon and laminae age models. We used the Bacon software (Blaauw and Christen, 2011), which applies a stepwise auto-regressive Gamma process to generate the final chronologies. By using Bacon, the final chronology for the entire Pu17, derived from the radiocarbon age model for the top 13 mm and the lamina-based chronology for the whole stalagmite (50 mm), was constructed. The final age model for the top 40 mm of Nu16 was also achieved, based on the radiocarbon chronology for the top 28 mm and the laminae-counting age model for the growth interval of 0–40 mm.

4. Results

The lamina-based chronology of Pu17 was discussed in Faraji et al. (2021) and is shown in Fig. 2. Following the same methodology, we constructed a chronology for Nu16 based on lamina counting (see Fig. 2) in the absence of LA-ICP-MS trace elements and without age constraints because U–Th age uncertainties are substantially large and are not useful. The laminae chronology was built by assuming the annual nature of laminae and assigning the age of retrieval to the topmost lamina, given that Nu16 was active when collected from the cave. The laminae age model reveals that the top 13 mm of Pu17, where radiocarbon analysis was also conducted, grew for 92 years from 1927 to 2019 CE (Faraji et al., 2021) with a mean growth rate of 132 ± 14 μm/year. The top 28 mm of Nu16 grew for 76 years from 1942 to 2018 CE with a mean growth rate of 313 ± 39 μm/year. No apparent growth interruptions were detected for neither Pu17 nor Nu16.

The AMS ^{14}C results are listed in Table 1 and illustrated in Fig. 3. The ^{14}C content in Pu17 is ≈ 95 pMC at a depth (distance from the top; DFT) of 12.15 mm, then slightly increases to ≈96 pMC at a DFT of 9.45 mm.

Table 1
The AMS^{14}C results for Pu17 and Nu16.

Lab ID (ANSTO Code)	Sample ID	DFT (mm)	$^{14}C \pm 1\sigma$ (pMC)	$\delta^{13}C$ (‰ VPDB)
		Pu17		
OZZ139	Pu17- 1	0.15	104.14 ± 0.26	−11.8
OZZ140	Pu17- 2	1.05	105.96 ± 0.28	−11.7
OZZ141	Pu17- 3	2.55	108.34 ± 0.30	−12.7
OZZ142	Pu17- 4	3.75	110.66 ± 0.26	−11.8
OZZ143	Pu17- 5	4.35	111.19 ± 0.27	−14.8
OZZ144	Pu17- 6	4.65	113.34 ± 0.28	−14.4
OZZ145	Pu17- 7	5.25	116.59 ± 0.28	−13.3
OZZ146	Pu17- 8	5.85	118.36 ± 0.28	−14.2
OZZ147	Pu17- 9	6.45	124.42 ± 0.30	−12.6
OZZ148	Pu17- 10	7.05	128.72 ± 0.34	−12.9
OZZ149	Pu17- 11	7.35	128.52 ± 0.28	−13.5
OZZ150	Pu17- 12	7.65	129.47 ± 0.32	−13.2
OZZ151	Pu17- 13	7.95	129.79 ± 0.28	−13.5
OZZ152	Pu17- 14	8.85	103.85 ± 0.26	−12.2
OZZ155	Pu17- 15	9.45	96.23 ± 0.25	−11.6
OZZ156	Pu17- 16	10.05	94.99 ± 0.27	−11.6
OZZ153	Pu17- 17	10.35	95.46 ± 0.29	−11.8
OZZ154	Pu17- 18	12.15	95.08 ± 0.23	−12.3
		Nu16		
OZZ157	Nu16-1	0.15	103.78 ± 0.28	−12.8
OZZ158	Nu16-2	2.85	105.96 ± 0.31	−9.0
OZZ159	Nu16-3	5.55	109.63 ± 0.32	−8.7
OZZ160	Nu16-4	8.25	116.48 ± 0.30	−8.1
OZZ161	Nu16-5	8.85	117.96 ± 0.31	−11.1
OZZ162	Nu16-6	9.45	119.53 ± 0.31	−11.1
OZZ163	Nu16-7	10.05	120.10 ± 0.31	−9.1
OZZ164	Nu16-8	10.65	124.01 ± 0.31	−11.0
OZZ165	Nu16-9	11.25	126.77 ± 0.26	−12.4
OZZ166	Nu16-10	11.55	125.00 ± 0.26	−8.6
OZZ167	Nu16-11	12.15	128.73 ± 0.37	−10.0
OZZ168	Nu16-12	13.05	130.43 ± 0.35	−8.6
OZZ844	Nu16-13	14.10	133.49 ± 0.31	−9.1
OZZ845	Nu16-14	15.30	133.80 ± 0.37	−11.1
OZZ849	Nu16-15	15.60	133.99 ± 0.36	−10.9
OZZ846	Nu16-16	16.20	134.44 ± 0.36	−11.0
OZZ847	Nu16-17	16.80	125.20 ± 0.35	−9.5
OZZ848	Nu16-18	19.72	102.12 ± 0.28	−10.1
OZY391	Nu16-19	20.10	99.00 ± 0.32	−9.8
OZY392	Nu16-20	21.00	96.47 ± 0.32	−9.1
OZY393	Nu16-21	21.90	95.64 ± 0.31	−9.3
OZY394	Nu16-22	23.10	94.54 ± 0.31	−9.3
OZY395	Nu16-23	24.00	94.23 ± 0.30	−10.1
OZY396	Nu16-24	26.10	95.12 ± 0.30	−9.1

The pMC continues rising until it reaches a maximum value of ≈130 pMC at 7.95 mm DFT. The ^{14}C content then fluctuates from 128 to 129 pMC between 7.65 and 7.05 mm DFT, after which it starts decreasing, to a value of ≈104 pMC at the top of Pu17. For Nu16, its ^{14}C content is ≈ 95 pMC at 26.1 mm DFT. The pMC varies around 94–95 between 26 and 21.9 mm DFT, then begins to rise at 21 mm, and reaches a maximum value of ≈134 at 16.2 mm DFT. The ^{14}C content then fluctuates around 133–134 pMC between 15.6 and 14 mm and declines to ≈103 pMC at the top of the stalagmite.

Chronological anchor points must first be assigned to build an age-depth model for Pu17 using the bomb pulse soil continuum method (Markowska et al., 2019). The first anchor point is based on the 'inflection point' (IP), calculated as the mean pMC of two radiocarbon samples, the ^{14}C sample where ^{14}C first appears to rise off the baseline and the closest baseline measurement. There were two possibilities for the choice of the IP, either from samples Pu17-14 and −15 (DFT 9.15 mm) or from Pu17-16 and −17 (DFT 9.75 mm), where we observed pMC values rising above the baseline values and hence the onset of bomb radiocarbon being incorporated in the speleothem. The second anchor point used was the extraction date as Pu17 was active when retrieved (Faraji et al., 2021). The age of 2019 CE was assigned to the top of the stalagmite. The date of retrieval and the IP were used as anchor points for the age-depth modelling. The correlation (r^2) between the modelled

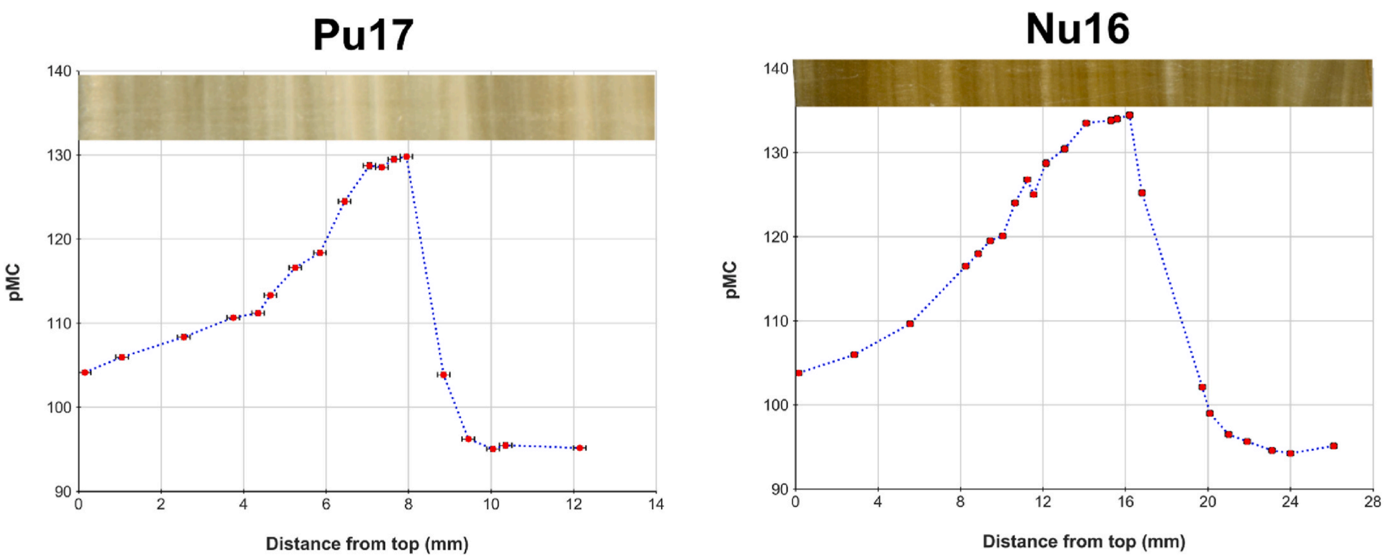

Fig. 3. The ^{14}C content in pMC (percent Modern Carbon) of the samples taken from Pu17 and Nu16 (bottom panels), and the speleothem scans of the portions analyzed for ^{14}C (top panels).

data and the measured data (actual) was highest for the age model IP = 9.15 mm, using 1956 CE as the IP year ($r^2 = 0.99$) (Fig. 4). This suggests a rapid transfer of the atmospheric ^{14}C to the stalagmite calcite in less than one year, given the onset of atmospheric bomb radiocarbon in the SH was in early 1956 (Hua et al., 2013). The age model indicates the bomb peak recorded in sample Pu-17-13 had an age of 1966 CE, also suggesting negligible time delay in the transfer of atmospheric ^{14}C signal to the stalagmite as atmospheric ^{14}C bomb peak in the SH occurred in 1965 CE (Fig. 5). Moreover, the carbon modelling indicates that 20% of the C reservoir comes from an instantaneous source, labelled C_1 in Table 2. It is, therefore, reasonable to infer an exceptionally fast transfer of atmospheric ^{14}C to Pu17. The age-depth model obtained through the radiocarbon yields a growth rate of 144 ± 8 μm/year for the top of 13 mm of Pu17.

For Nu16, the IP was determined to be between samples Nu16-20 and 21 (DFT 21.45 mm). The r^2 value between the modelled and actual data was 0.97, using 1957 CE as the IP year (onset of the bomb pulse) (Fig. 4). This suggests that there is a slower transfer of the atmospheric carbon signal to Nu16 than that for Pu17. Stalagmite Nu16 was retrieved from the cave in 2018 and was still active. Thus, the age of the stalagmite tip (2018 CE) and the IP were anchor points for age modelling. The Nu16 bomb pulse peak occurs in 1972 CE, within the sample Nu16-16 (Fig. 5). The modelling suggests contributions predominately from C_2 and C_3, with no contribution from C_1 or C_4 (Table 2). Having no contribution from a C_1 reservoir also supports that Nu16 may have a slower transfer of atmospheric carbon to the stalagmite than Pu17, and consequently a later bomb peak. The less negative δ^{13}C values, presented in Table 1, in Nu16 (mean = −10.1 ± 1.3‰ VPDB, n = 18) compared to Pu17 (mean = −12.8 ± 0.9‰ VPDB, n = 24) could be indicative of longer water-host rock interaction times and a slower transmissivity of rain signal to Nu16 compared to Pu17 (Table 1). The average DCP value for Nu16 of 2.7% is similar to the DCP value for Pu17 (Table 2). The age-depth model yields a growth rate of 347 ± 10 μm/year for the top 28 mm of Nu16, which is much higher than that of Pu17.

As listed in Table 2, Pu17 has a 21% contribution from a very fast turnover C reservoir (C_1) which is consistent with the measured data showing a sharp ^{14}C rise from the baseline and an early stalagmite bomb

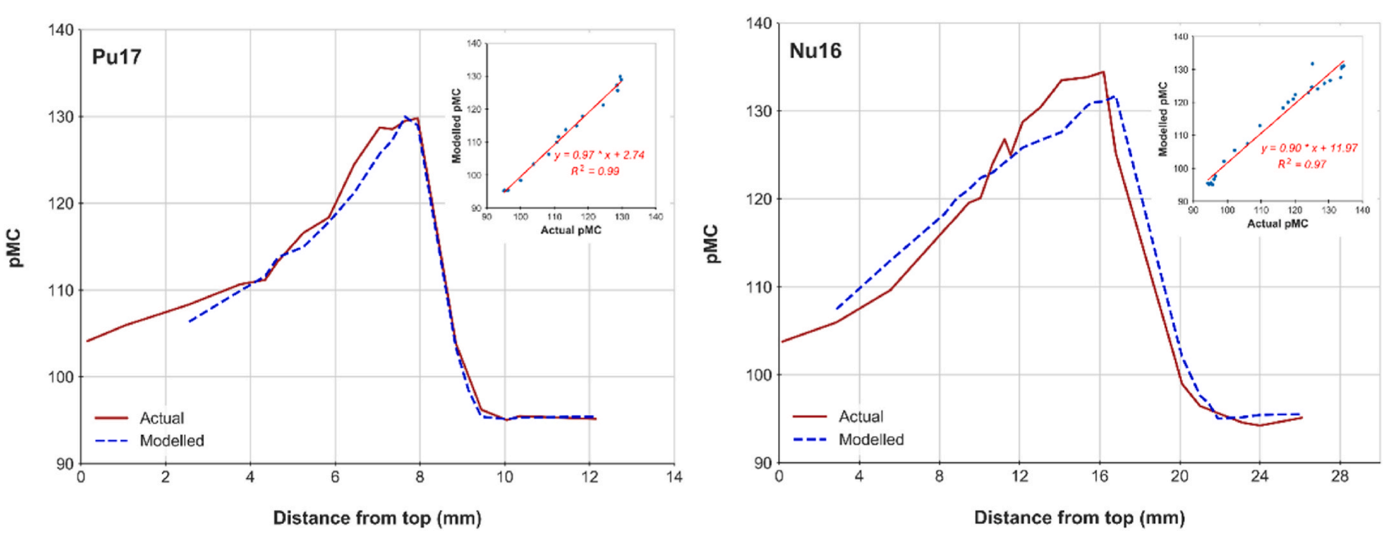

Fig. 4. Age-depth modelling for Pu17 and Nu16 using bomb pulse soil continuum method from Markowska et al. (2019). Brown curves show the actual (measured) ^{14}C data, and blue dashed curves are modelled ^{14}C data. The correlation (r^2) between actual and modelled data is 0.99 for Pu17 and 0.97 for Nu16 (see insert diagrams).

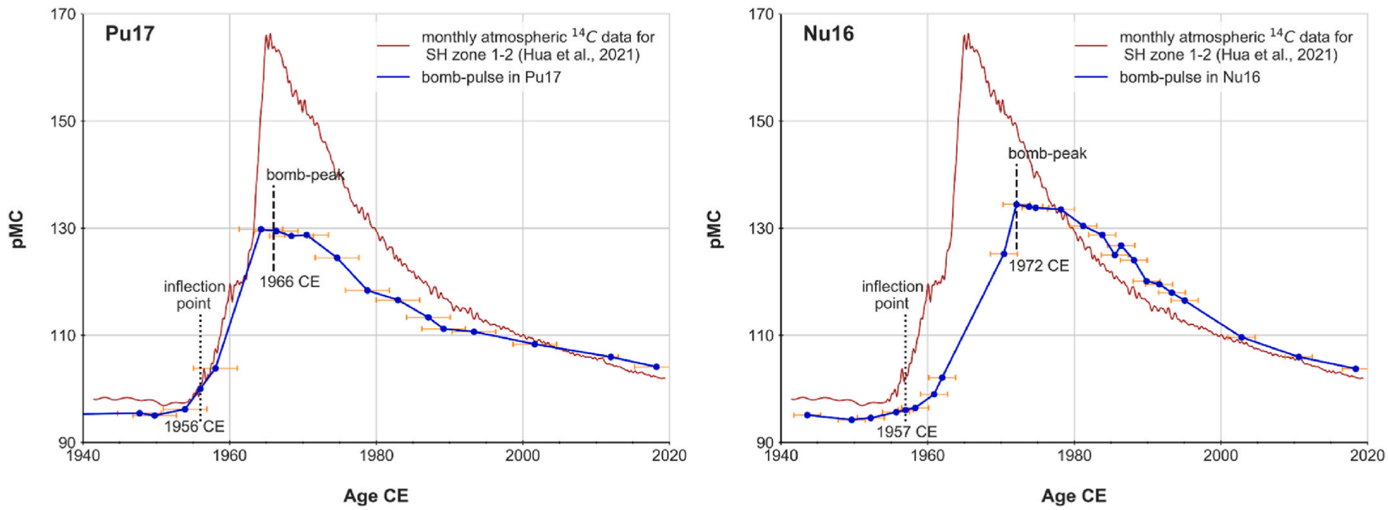

Fig. 5. Bomb pulse modelling for Pu17 and Nu16. Brown curves show monthly atmospheric ^{14}C data for the Southern Hemisphere Zone 1–2 (Hua et al., 2021), and blue curves show the modelled ages for these stalagmites. The onset (inflection point) and the peak of the bomb pulse recorded in the stalagmites are shown. Pu17 shows a sharp and early bomb peak in 1966 CE, whereas Nu16 depicts a later bomb peak in 1972 CE, indicating a slower transfer of atmospheric radiocarbon to the stalagmite.

Table 2
Model output from C modelling shows the contributions (%) from each C reservoir and average DCP values.

Speleothem	Modelled contribution (%) from each *C* reservoir				Average DCP (%) ±1SD
	F (C_1)	F (C_2)	F (C_3)	F (C_4)	
Pu17	21	33	13	32	2.11 ± 0.47
Nu16	0	57	43	0	2.71 ± 0.55

peak. On the other hand, Nu16 has no contribution from the instantaneous C pool, which results in a longer lag between the timing of the atmospheric bomb peak and that recorded in the stalagmite. Very low DCP values for both Pu17 and Nu16 account for the relatively high bomb peak values (ca. 130 and 134 pMC for Pu17 and Nu16, respectively) (see Fig. 5), which allows reconstructing accurate radiocarbon chronologies for these two stalagmites.

5. Discussion

5.1. *Comparison between the bomb curves reported in this study and those in the literature*

Comparing the radiocarbon age models of Pu17 and Nu16 with other published radiocarbon chronologies for stalagmites in the SH and the South Pacific show that Pu17 has the earliest bomb peak. In addition, both Pu17 and Nu16 record sharp rises in ^{14}C after the bomb onsets with clearly defined bomb peaks (Fig. 6). Nu16 shows the highest peak pMC value (134.4) recorded in modern SH speleothems, being slightly higher than that in stalagmite WM4 (134.1) from the Wombeyan Caves (Hodge et al., 2011). This is likely due to the minimal overburden (2–8 m) and the sparse soil cover in Atiu that in some areas, only tree litter is present. The most similar bomb-pulse radiocarbon curve to Pu17 and Nu16 was reported from semi-arid Wellington Caves in southeast Australia (stalagmite WB; Markowska et al. (2019)), where the overburden is 25 m but has limited soil cover and exposed bedrock (less than 0.3 m). Bomb-pulse curves recorded in speleothems from Liang Luar cave in Indonesia (Griffiths et al., 2012), Cold Air cave in South Africa (Sundqvist et al., 2013) and Careys Cave in Australia (Scroxton et al., 2021) are very different from those from Atiu with much-damped bomb ^{14}C rising and much lower bomb peak values (Fig. 6). That is likely

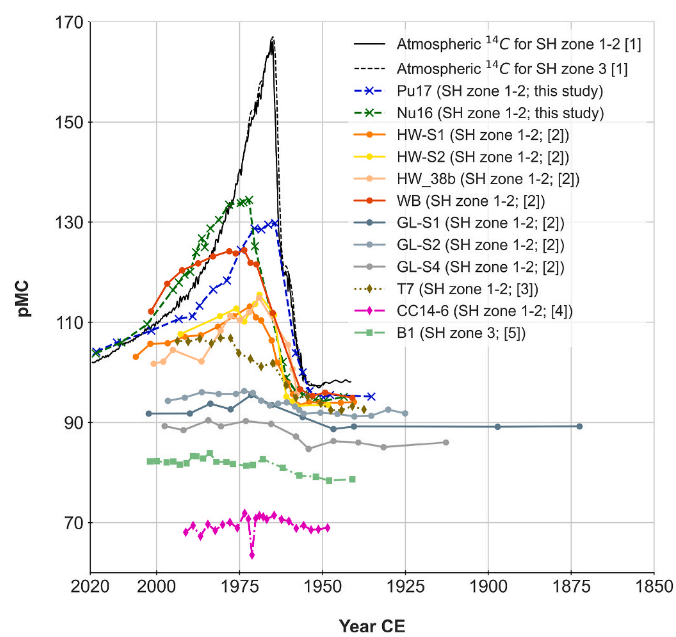

Fig. 6. Some of the published bomb radiocarbon chronologies for speleothems in the SH compared with those recorded in Pu17 and Nu16, and SH atmospheric ^{14}C data. [1] - Hua et al. (2021), [2] - Markowska et al. (2019), [3] - Sundqvist et al. (2013), [4] - Scroxton et al. (2021), and [5] - Griffiths et al. (2012).

related to the site-specific soil and host rock; since Liang Luar cave is buried under a thick rock burden (30–50 m) and soil cover (1–2 m), the bomb peak recorded in stalagmite B1 of this cave is not clear as that reported for stalagmite T7 of the Cold Air cave with a 20 m thick overburden and less than 0.3 m soil. Similarly, Careys Cave has an overburden of 30 m and a very damped bomb ^{14}C. Therefore, the sharp and clear ^{14}C in the Atiuan stalagmites provide excellent age models, paving the way to construct annual records of hydroclimate. Additionally, with Pu17 having the shortest delay relative to the atmospheric bomb peak, and Nu16 showing the highest peak pMC value compared to over 20 published stalagmites (Borsato et al., 2022; Markowska et al., 2019), Atiuan stalagmites would provide an excellent reference section for the Anthropocene series, as discussed by Borsato et al. (2022).

5.2. Radiocarbon vs laminae chronologies, and the final chronologies

Chronologies based on counting physical and chemical laminae indicate that the top 13 mm of Pu17 grew for 92 years from 1927 to 2019 CE (Faraji et al., 2021), and the top 28 mm of Nu16 grew for 76 years from 1942 to 2018 CE. These suggest a mean growth rate of 132 ± 14 μm/year for Pu17 and 313 ± 39 μm/year for Nu16. The radiocarbon chronologies indicate slightly different growth rates for the top 13 mm of Pu17 (89 ± 3 years; 146 ± 5 μm/year) and the top 28 mm of Nu16 (78 ± 2 years; 358 ± 8 μm/year).

The age-depth relationship generated by radiocarbon modelling follows a constant annual growth for Pu17 and Nu16, while those obtained by laminae counting show variable annual growth rates. This explains why the laminae counting chronologies and those obtained through radiocarbon modelling are not the same. As shown in Fig. 7, whilst the 1σ uncertainty ranges of laminae counting age models encompass those associated with the bomb-pulse models, the difference between the two approaches can be up to nine years for Pu17 and three years for Nu16 within the growth interval. Interestingly, the laminae age models almost always overestimated the age of the stalagmites for at least 2–3 years (Fig. 7). However, for most of the growth interval, the offset between the chronologies is around 2–3 years for both stalagmites, which falls within the 1σ uncertainty ranges of the age models (Fig. 7).

In order to construct the final chronologies for the entire growth interval of Pu17 (50 mm) and the top 40 mm of Nu16, the radiocarbon and laminae chronologies were spliced for each stalagmite. For the top parts of the stalagmites where the radiocarbon and laminae age models overlap, the final chronologies are closer to the radiocarbon age model than to the laminae counting because radiocarbon has smaller uncertainties than the initial laminae age model both in Pu17 (±3 vs ± 11 years) and Nu16 (±2 vs ± 6 years). Fig. 8 shows the final chronologies constructed for Pu17 and Nu16. As shown in the figure, the top 13 mm of Pu17 and top 28 mm of Nu16, where radiocarbon samples were collected, have narrower ranges of age uncertainties compared to the deeper parts. According to the final chronologies, stalagmite Pu17 grew for 347 years from 1672 to 2019 CE with an average growth rate of 144 ± 5 μm/year, and the top 40 mm of stalagmite Nu16 grew for 130 years from 1888 to 2018 CE with a mean growth rate of 307 ± 13 μm/year.

5.3. Implications for regional hydroclimate

In order to demonstrate the significance of the chronologies constructed via combining the radiocarbon dating with laminae counting, we use the Pu17 hydroclimate proxies which were initially discussed in Faraji et al. (2021). By analyzing a group of trace elements including Mg, Na, Sr, Ba through LA-ICP-MS, and then performing a principal component analysis (PCA), Faraji et al. (2021) argued that infiltration - rainfall minus potential evapotranspiration (PET) - is the mechanism controlling the concentration of trace elements in Pu17. They used the Thornthwaite formula (Thornthwaite, 1948) to calculate the PET for Atiu for 1914–2019. The calculated infiltration was then acquired by subtracting the PET from instrumental rainfall data. Faraji et al. (2021) showed that principal component one (PC1) of the PCA, including Mg, Na, Sr, Ba that accounts for 42% variance in the trace elements, correlates positively with infiltration (and thus rainfall). As such, the more positive values of PC1 should correspond to higher infiltration, whilst its negative values should coincide with lower infiltration. In Fig. 9, the PC1 is compared with the calculated infiltration in Atiu by using both the laminae chronology (Fig. 9a) and the final chronology constructed in this study (Fig. 9b). In both cases, PC1 follows the variation in infiltration and more positive values of PC1 point to higher infiltration. However, when PC1 was plotted using the final age model developed in this study, it showed a much clear relationship with infiltration with a higher correlation coefficient ($r = 0.20$) than when plotted using the laminae age model ($r = 0.13$). This corroborates the idea that infiltration is the overarching mechanism controlling the variability of trace elements in Pu17, even though each element might originate from a different source Faraji et al. (2021). This also reveals the excellent potential of speleothems from the Cook Islands to provide reliable information, at least, on the historical variability of the El Niño Southern Oscillation (ENSO). That is because the ENSO, represented by Southern Oscillation Index (SOI) in Fig. 9c, drives much of the interannual variation in rainfall (and thus infiltration) in the Pacific Islands (Weir et al., 2021). El Niño events are generally associated with relatively dry periods and less rainfall in the southern Cook Islands, whereas La Niña events mark wet periods (see Fig. 9c). Precisely-dated high-resolution proxies of infiltration - for example, PC1 in Pu17 - are excellent material for reconstructing infiltration over the past, at least a few hundred years, that can cast some

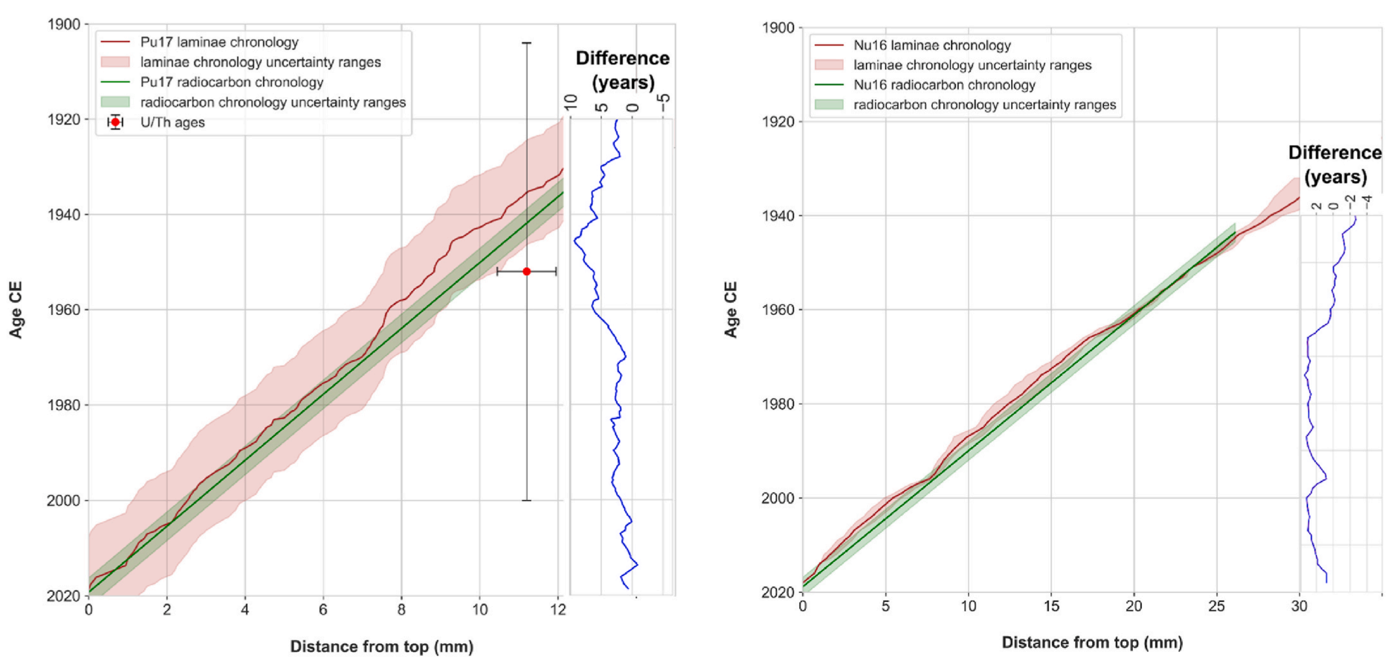

Fig. 7. Comparison of the laminae counting chronology constructed for Pu17 (Faraji et al., 2021) and Nu16 with corresponding radiocarbon chronologies. The offset between the laminae and radiocarbon age models (blue curve) is mostly around 2–3 years, which falls within the age models' 1σ uncertainty ranges.

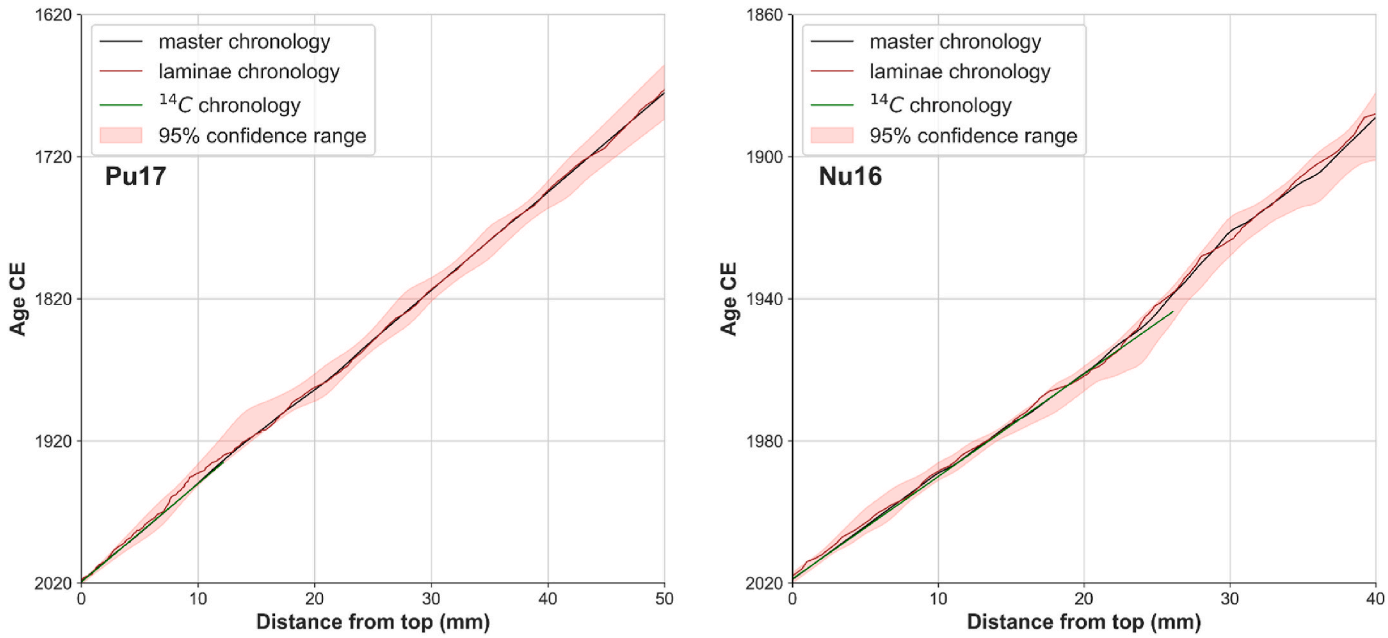

Fig. 8. The final constructed chronologies (black curve) for Pu17 and Nu16 after splicing the radiocarbon (green curve) and laminae age models (brown curve) by using the Bacon age-depth modelling (Blaauw and Christen, 2011). The 95% confidence ranges were produced by Bacon and are shown in red envelopes.

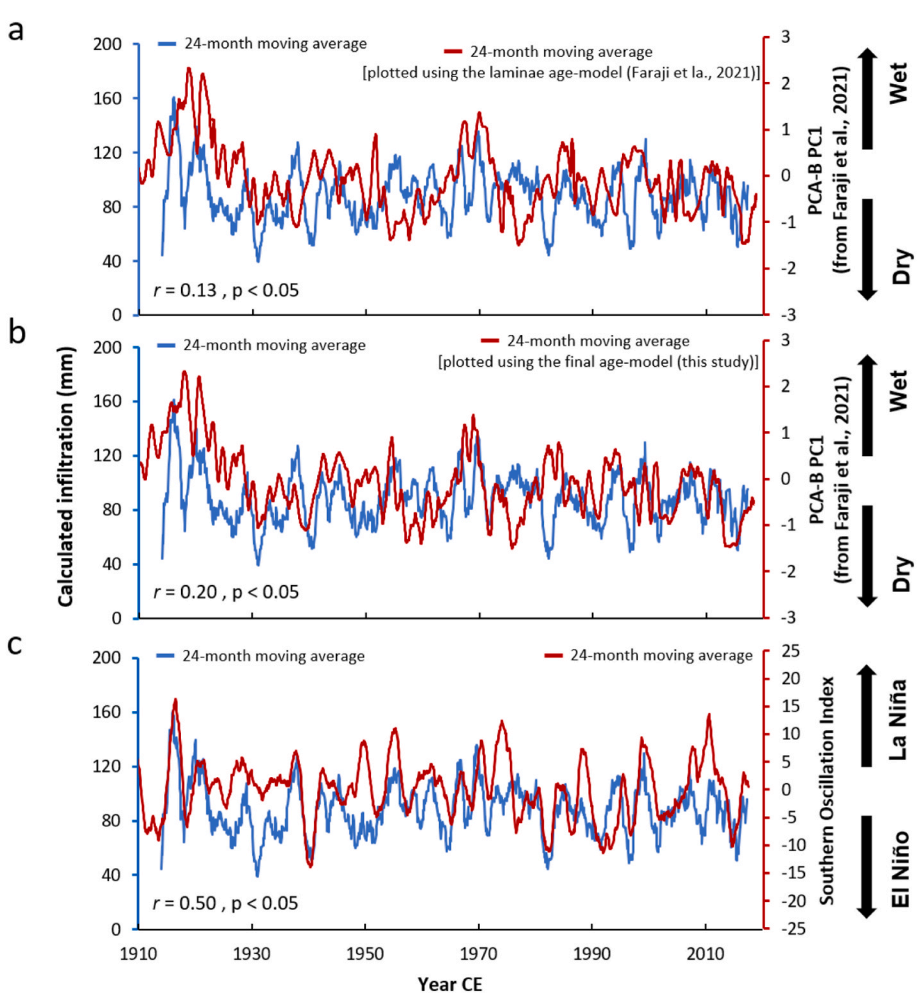

Fig. 9. The laminae age model (a) and the final chronology constructed in this study (b) in comparison with the PC1 - of PCA-B in Faraji et al. (2021) - as a hydroclimate proxy with the calculated infiltration. In both cases, PC1 follows the variation in infiltration, and more positive values of PC1 correspond to higher infiltration (wet) and vice versa. However, when PC1 was plotted using the age model developed in this study, it showed a far more clear relationship with infiltration (b) than when plotted using the laminae age model (a). The calculated infiltration is also plotted against the Southern Oscillation Index (representing ENSO), showing a strong link between dry (wet) periods and El Niño (La Niña) events. The instrumental record for SOI was acquired from the Australian Bureau of Meteorology website at: http://www.bom.gov.au/.

light on the past variation of rainfall driven by ENSO. This becomes even more important in the Pacific Islands region, where water for agriculture is almost entirely supplied by rainfall rather than by irrigation systems (Barnett, 2011).

Therefore, it is clear that joint use of bomb radiocarbon and laminae counting chronologies has improved the fit between the calculated infiltration and the PC1 data, paving the way towards obtaining well-dated climate records from Atiuan stalagmites. The combined chronology has improved the accuracy and precision of the age model in the very young parts of the stalagmites, which are otherwise hard to date due to significant uncertainties of U/Th dating and also complexities in the fabrics and possible occurrence of sub-annual laminae. Faraji et al. (2021) were able to decrease the uncertainty of U/Th chronology by 45% via counting visible physical and chemical laminae. However, that laminae age model still had some 4% uncertainty. The final constructed chronology developed in this study further constrained the age model for Pu17 by reducing the uncertainty for the top 13 mm of the stalagmite by 3%. The final chronology for Nu16 has only 2% uncertainty in the top 28 mm and up to 4% at DFT 40 mm. In Fig. 10, time series of $\delta^{18}O$ values for Pu17 and Nu16 (Faraji et al., 2022) are plotted using chronologies constructed in this study. It is clear from Fig. 10 that the two stalagmites show similar $\delta^{18}O$ patterns over the overlapped interval, thus confirming the reliability of constructed age models.

Therefore, even though speleothems from the tropical South Pacific commonly suffer from large uncertainties in their U–Th dating, the use of our combined chronological approach allows us to reduce dating uncertainty and examine paleoclimate records at annual resolution. That is because these speleothems usually benefit from a rapid transmissivity of rainfall in shallow caves with a porous or fractured host rock. Additionally, little soil cover or tree litter further facilitates transmissivity. This, in an environment with seasonal contrast in precipitation (or in cave ventilation/breathing), could potentially lead to the development of both physical and chemical annual laminae in speleothems. Using the combined approach of ^{14}C modelling and visible and chemical laminae counting for tropical Pacific examples can improve the accuracy of dating tremendously, as was shown in this study. This opens up the possibility of obtaining annually resolved hydroclimate records that advances knowledge about pre-instrumental hydroclimate variability in the tropical South Pacific and reduces uncertainties about the magnitude, frequency and duration of past droughts and pluvials.

6. Conclusion

Two stalagmites from Southern Cook Islands in the tropical South Pacific were dated using the ^{14}C bomb pulse soil continuum method from Markowska et al. (2019). Results indicate that the onset of the bomb-pulse in Pu17 starts in 1956 and reaches its bomb peak in 1966 CE. The carbon modelling also indicates a 20% contribution from C_1 - an instantaneous C source. These data suggest an exceptionally fast transfer of atmospheric carbon to the stalagmite <1 year, which was also supported by very negative $\delta^{13}C$ values in Pu17 (<-12‰ VPDB). The age-depth modelling for Nu16 was indicative of a slower transfer of atmospheric carbon to the stalagmite than Pu17, with a bomb radiocarbon onset and bomb peak in 1957 and 1972 CE, respectively. This was corroborated by less negative $\delta^{13}C$ values in Nu16 (−8 to −11‰) than Pu17 (−11 to −15‰), and also by the carbon modelling that points out no contribution from C_1 reservoirs.

The low DCP values (2–3%) in both Pu17 and Nu16, leading to their high bomb peak of 130–134 pMC, render such accurate radiocarbon chronologies possible. According to the radiocarbon chronologies constructed in this study, the top 13 mm of Pu17 grew for 89 years (1930–2019 CE) with a constant growth rate of 144 μm/year. The top 28 mm of Nu16 grew for 78 years (1940–2018 CE) with a rate more than double that of Pu17, around 347 μm/year. The radiocarbon chronologies and available laminae counting age models were then spliced to achieve a single master chronology for each stalagmite. The final age models suggest that Pu17 grew for 347 years from 1672 to 2019 CE, and the top 40 mm of the stalagmite Nu16 grew for 130 years from 1888 to 2018 CE.

Based on the final constructed chronology, we compared the already published Pu17 proxies of hydroclimate with the calculated infiltration record in Atiu, which showed great agreement between the two series. This supports the accuracy of the final age-depth model. This also attests to the great potential of Pu17, and likely Nu16 as well, to advance knowledge about pre-instrumental hydroclimate variability in the tropical South Pacific. This study is an example of ^{14}C age modelling combined with visible physical and chemical laminae counting and how it can improve the accuracy of dating for otherwise hard-to-date tropical Pacific speleothems. Such accurate and precise chronologies allow obtaining robust paleoclimate records for the climate-vulnerable South Pacific Island communities through enhancing the quality of the calibration of climate proxy data with the current and instrumental weather parameters measured at both cave surface and interior.

Declaration of competing interest

The authors declare that they have no known competing financial interests or personal relationships that could have appeared to influence the work reported in this paper.

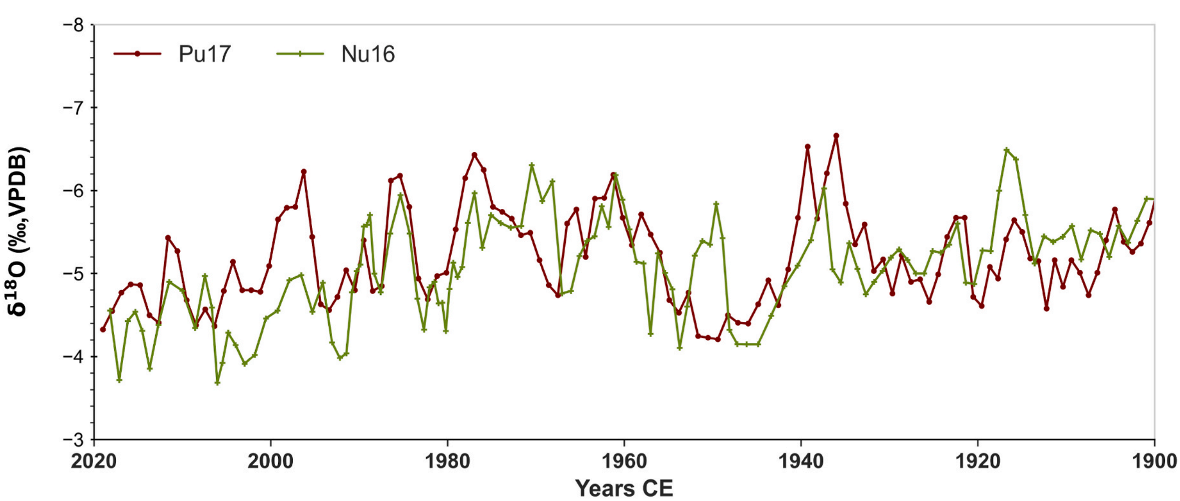

Fig. 10. Time series of Pu17 and Nu16 (Faraji et al., 2022) plotted using chronologies constructed in this study.

Data availability

Data will be made available on request.

Acknowledgements

Special thanks to the landowners, people and Island Council, and to the National Research Committee of the Cook Islands for permission to explore the caves of Atiu and take samples, and to Tura Koronui and George Mateariki, who introduced us to the caves in Atiu. The radiocarbon analysis was carried out at ANSTO. This study was supported by the Australian Research Council Discovery Project grant DP160101058. M.F. was supported by the Australian Government through an "Australian Government Research Training Program Scholarship" and was also supported by The Australian Institute of Nuclear Science and Engineering through a Postgraduate Research Award (award ALN-STU12486). We would also like to thank the editor and anonymous reviewers for their constructive comments and suggestions that greatly improved the quality of this manuscript.

References

Bajo, P., Borsato, A., Drysdale, R., Hua, Q., Frisia, S., Zanchetta, G., Hellstrom, J., Woodhead, J., 2017. Stalagmite carbon isotopes and dead carbon proportion (DCP) in a near-closed-system situation: an interplay between sulphuric and carbonic acid dissolution. Geochem. Cosmochim. Acta 210, 208–227. https://doi.org/10.1016/j.gca.2017.04.038.

Baker, A., C Hellstrom, J., Kelly, B.F.J., Mariethoz, G., Trouet, V., 2015. A composite annual-resolution stalagmite record of North Atlantic climate over the last three millennia. Sci. Rep. 5, 10307 https://doi.org/10.1038/srep10307.

Baker, A., Mariethoz, G., Comas-Bru, L., Hartmann, A., Frisia, S., Borsato, A., Treble, P. C., Asrat, A., 2021. The properties of annually laminated stalagmites-A global synthesis. Rev. Geophys. 59 (2) https://doi.org/10.1029/2020RG000722 e2020RG000722.

Ban, F., Baker, A., Marjo, C.E., Duan, W., Li, X., Han, J., Coleborn, K., Akter, R., Tan, M., Nagra, G., 2018. An optimized chronology for a stalagmite using seasonal trace element cycles from Shihua Cave, Beijing, North China. Sci. Rep. 8 (1), 4551. https://doi.org/10.1038/s41598-018-22839-z.

Bar-Matthews, M., Ayalon, A., Kaufman, A., Wasserburg, G.J., 1999. The Eastern Mediterranean paleoclimate as a reflection of regional events: soreq cave, Israel. Earth Planet Sci. Lett. 166 (1), 85–95. https://doi.org/10.1016/S0012-821X(98)00275-1.

Barnett, J., 2011. Dangerous climate change in the Pacific Islands: food production and food security. Reg. Environ. Change 11 (1), 229–237. https://doi.org/10.1007/s10113-010-0160-2.

Beck, J.W., Richards, D.A., Lawrence, R., Edwards Silverman, B.W., Smart, P.L., Donahue, D.J., Hererra-Osterheld, S., Burr, G.S., Calsoyas, L., Timothy, A.J., Jull, Biddulph, D., 2001. Extremely large variations of atmospheric 14C concentration during the last glacial period. Science 292 (5526), 2453–2458. https://doi.org/10.1126/science.1056649.

Blaauw, M., Christen, J.A., 2011. Flexible paleoclimate age-depth models using an autoregressive gamma process. Bayesian Analysis 6 (3), 457–474. https://doi.org/10.1214/11-BA618, 418.

Borsato, A., Frisia, S., Fairchild, I.J., Somogyi, A., Susini, J., 2007. Trace element distribution in annual stalagmite laminae mapped by micrometer-resolution X-ray fluorescence: implications for incorporation of environmentally significant species. Geochem. Cosmochim. Acta 71 (6), 1494–1512. https://doi.org/10.1016/j.gca.2006.12.016.

Borsato, A., Frisia, S., Fairchild, I.J., Wynn, P., Fohlmeister, J., 2022. The Ernesto Cave, Northern Italy, as a Candidate Auxiliary Reference Section for the Definition of the Anthropocene Series: *Anthropocene Review* (in press).

Borsato, A., Frisia, S., Howard, D., Greig, A., 2021. A Guide to Synchrotron Hard X-Ray Fluorescence Mapping of Annually Laminated Stalagmites: Sample Preparation, Analysis and Evaluation: *Spectrochimica Acta Part B: Atomic Spectroscopy*, 106308.

Bruce, J.G., 1983. Patterns and classification by soil taxonomy of the soils of the southern Cook Islands. Geoderma 31 (4), 301–323. https://doi.org/10.1016/0016-7061(83)90043-5.

Cai, W., Santoso, A., Wang, G., Yeh, S.-W., An, S.-I., Cobb, K.M., Collins, M., Guilyardi, E., Jin, F.-F., Kug, J.-S., Lengaigne, M., McPhaden, M.J., Takahashi, K., Timmermann, A., Vecchi, G., Watanabe, M., Wu, L., 2015. ENSO and greenhouse warming. Nat. Clim. Change 5 (9), 849–859. https://doi.org/10.1038/nclimate2743.

Carlson, P.E., Banner, J.L., Johnson, K.R., Casteel, R.C., Breecker, D.O., 2019. Carbon cycling of subsurface organic matter recorded in speleothem 14C records: maximizing bomb-peak model fidelity. Geochem. Cosmochim. Acta 246, 436–449. https://doi.org/10.1016/j.gca.2018.11.035.

Dorale, J.A., Edwards, R.L., Alexander, E.C., Shen, C.-C., Richards, D.A., Cheng, H., 2004. Uranium-Series Dating of Speleothems: Current Techniques, Limits, & Applications. Springer US, Boston, MA, pp. 177–197.

Fairchild, I.J., Baker, A., 2012. Speleothem Science: from Process to Past Environments. John Wiley & Sons.

Faraji, M., Borsato, A., Frisia, S., Hellstrom, J.C., Lorrey, A., Hartland, A., Greig, A., Mattey, D.P., 2021. Accurate dating of stalagmites from low seasonal contrast tropical Pacific climate using Sr 2D maps, fabrics and annual hydrological cycles. Sci. Rep. 11 (1), 2178. https://doi.org/10.1038/s41598-021-81941-x.

Faraji, M., Borsato, A., Frisia, S., Mattey, D.P., Drysdale, R.N., Verdon-Kidd, D.C., Malcolm, R., Marca, A., 2022. Controls on rainfall variability in the tropical South Pacific for the last 350 years reconstructed from oxygen isotopes in stalagmites from the Cook Islands. Quat. Sci. Rev. 289, 107633 https://doi.org/10.1016/j.quascirev.2022.107633.

Fink, D., Hotchkis, M., Hua, Q., Jacobsen, G., Smith, A.M., Zoppi, U., Child, D., Mifsud, C., van der Gaast, H., Williams, A., Williams, M., 2004. The ANTARES AMS facility at ANSTO. Nucl. Instrum. Methods Phys. Res. Sect. B Beam Interact. Mater. Atoms 223, 109–115. https://doi.org/10.1016/j.nimb.2004.04.025.

Fisher, L.A., Fougerouse, D., Cleverley, J.S., Ryan, C.G., Micklethwaite, S., Halfpenny, A., Hough, R.M., Gee, M., Paterson, D., Howard, D.L., Spiers, K., 2015. Quantified, multi-scale X-ray fluorescence element mapping using the Maia detector array: application to mineral deposit studies. Miner. Deposita 50 (6), 665–674. https://doi.org/10.1007/s00126-014-0562-z.

Fohlmeister, J., Kromer, B., Mangini, A., 2011. The Influence of Soil Organic Matter Age Spectrum on the Reconstruction of Atmospheric 14C Levels via Stalagmites, vol. 53, pp. 99–115. https://doi.org/10.1017/s003382220003438x, 1.

Frisia, S., Borsato, A., Hartland, A., Faraji, M., Demeny, A., Drysdale, R.N., Marjo, C.E., 2022. Crystallization pathways, fabrics and the capture of climate proxies in speleothems: examples from the tropics. Quat. Sci. Rev. 297, 107833 https://doi.org/10.1016/j.quascirev.2022.107833.

Genty, D., Massault, M., 1999. Carbon transfer dynamics from bomb-14C and δ13C time series of a laminated stalagmite from SW France—modelling and comparison with other stalagmite records. Geochem. Cosmochim. Acta 63 (10), 1537–1548. https://doi.org/10.1016/S0016-7037(99)00122-2.

Goslar, T., Hercman, H., Pazdur, A., 2000. Comparison of U-Series and Radiocarbon Dates of Speleothems, vol. 42, pp. 403–414. https://doi.org/10.1017/s0033822200030332, 3.

Griffiths, M.L., Fohlmeister, J., Drysdale, R.N., Hua, Q., Johnson, K.R., Hellstrom, J.C., Gagan, M.K., Zhao, J.x., 2012. Hydrological control of the dead carbon fraction in a Holocene tropical speleothem. Quat. Geochronol. 14, 81–93. https://doi.org/10.1016/j.quageo.2012.04.001.

Harmon, R.S., Ford, D.C., Schwarcz, H.P., 1977. Interglacial chronology of the Rocky and Mackenzie Mountains based upon 230Th–234U dating of calcite speleothems. Can. J. Earth Sci. 14 (11), 2543–2552. https://doi.org/10.1139/e77-220.

Held, I.M., Soden, B.J., 2006. Robust responses of the hydrological cycle to global warming. J. Clim. 19 (21), 5686–5699. https://doi.org/10.1175/jcli3990.1.

Hellstrom, J., 2003. Rapid and accurate U/Th dating using parallel ion-counting multi-collector ICP-MS. J. Anal. At. Spectrom. 18 (11), 1346. https://doi.org/10.1039/b308781f.

Hellstrom, J., 2006. U–Th dating of speleothems with high initial 230Th using stratigraphical constraint. Quat. Geochronol. 1 (4), 289–295. https://doi.org/10.1016/j.quageo.2007.01.004.

Hodge, E., McDonald, J., Fischer, M., Redwood, D., Hua, Q., Levchenko, V., Drysdale, R., Waring, C., Fink, D., 2011. Using the 14C bomb pulse to date young speleothems. Radiocarbon 53 (2), 345–357. https://doi.org/10.1017/S0033822200056605.

Holland, P., Olson, S., 1989. Introduced versus native plants in austral forests. Prog. Phys. Geogr.: Earth Environ. 13 (2), 260–293. https://doi.org/10.1177/030913338901300205.

Hua, Q., Barbetti, M., Rakowski, A.Z., 2013. Atmospheric radiocarbon for the period 1950–2010. Radiocarbon 55 (4), 2059–2072. https://doi.org/10.2458/azu_js_rc.v55i2.16177.

Hua, Q., Jacobsen, G.E., Zoppi, U., Lawson, E.M., Williams, A.A., Smith, A.M., McGann, M.J., 2001. Progress in radiocarbon target preparation at the ANTARES AMS Centre. Radiocarbon 43 (2A), 275–282. https://doi.org/10.1017/S003382220003811X.

Hua, Q., McDonald, J., Redwood, D., Drysdale, R., Lee, S., Fallon, S., Hellstrom, J., 2012. Robust chronological reconstruction for young speleothems using radiocarbon. Quat. Geochronol. 14, 67–80. https://doi.org/10.1016/j.quageo.2012.04.017.

Hua, Q., Turnbull, J.C., Santos, G.M., Rakowski, A.Z., Ancapichún, S., De Pol-Holz, R., Hammer, S., Lehman, S.J., Levin, I., Miller, J.B., Palmer, J.G., Turney, C.S.M., 2021. Atmospheric radiocarbon for the period 1950-2019. Radiocarbon 1–23. https://doi.org/10.1017/RDC.2021.95.

Jamieson, R.A., Baldini, J.U.L., Frappier, A.B., Müller, W., 2015. Volcanic ash fall events identified using principal component analysis of a high-resolution speleothem trace element dataset. Earth Planet Sci. Lett. 426, 36–45. https://doi.org/10.1016/j.epsl.2015.06.014.

Johnson, K., Hu, C., Belshaw, N., Henderson, G., 2006. Seasonal trace-element and stable-isotope variations in a Chinese speleothem: the potential for high-resolution paleomonsoon reconstruction. Earth Planet Sci. Lett. 244 (1), 394–407. https://doi.org/10.1016/j.epsl.2006.01.064.

Kirch, P.V., 2000. On the Road of the Winds: an Archaeological History of the Pacific Islands before the European Contact. University of California Press, Berkeley, California.

Li, H.-C., Ku, T.-L., You, C.-F., Cheng, H., Edwards, R.L., Ma, Z.-B., Tsai, W.-s., Li, M.-D., 2005. 87Sr/86Sr and Sr/Ca in speleothems for paleoclimate reconstruction in Central China between 70 and 280 kyr ago. Geochem. Cosmochim. Acta 69 (16), 3933–3947. https://doi.org/10.1016/j.gca.2005.01.009.

Markowska, M., Fohlmeister, J., Treble, P.C., Baker, A., Andersen, M.S., Hua, Q., 2019. Modelling the 14C bomb-pulse in young speleothems using a soil carbon continuum

model. Geochem. Cosmochim. Acta 261, 342–367. https://doi.org/10.1016/j.gca.2019.04.029.
Marshall, P., 1930. Geology of Rarotonga and Atiu, Bernice P. Bishop Museum Bulletin, p. 72.
Mattey, D., Lowry, D., Duffet, J., Fisher, R., Hodge, E., Frisia, S., 2008. A 53 year seasonally resolved oxygen and carbon isotope record from a modern Gibraltar speleothem: reconstructed drip water and relationship to local precipitation. Earth Planet Sci. Lett. 269 (1), 80–95. https://doi.org/10.1016/j.epsl.2008.01.051.
Meteorology, A.B.o., CSIRO, 2011. Climate Change in the Pacific: Scientific Assessment and New Research, vol. 2 (Country Reports).
Miorandi, R., Borsato, A., Frisia, S., Fairchild, I.J., Richter, D.K., 2010. Epikarst hydrology and implications for stalagmite capture of climate changes at Grotta di Ernesto (NE Italy): results from long-term monitoring. Hydrol. Process. 24 (21), 3101–3114. https://doi.org/10.1002/hyp.7744.
Nagra, G., Treble, P.C., Andersen, M.S., Bajo, P., Hellstrom, J., Baker, A., 2017. Dating stalagmites in mediterranean climates using annual trace element cycles. Sci. Rep. 7 (1), 621. https://doi.org/10.1038/s41598-017-00474-4.
Noronha, A.L., Johnson, K.R., Southon, J.R., Hu, C., Ruan, J., McCabe-Glynn, S., 2015. Radiocarbon evidence for decomposition of aged organic matter in the vadose zone as the main source of speleothem carbon. Quat. Sci. Rev. 127, 37–47. https://doi.org/10.1016/j.quascirev.2015.05.021.
Oriani, F., Treble, P.C., Baker, A., Mariethoz, G., 2022. WlCount: geological lamination detection and counting using an image analysis approach. Comput. Geosci. 160, 105037 https://doi.org/10.1016/j.cageo.2022.105037.
Orland, I.J., Burstyn, Y., Bar-Matthews, M., Kozdon, R., Ayalon, A., Matthews, A., Valley, J.W., 2014. Seasonal climate signals (1990–2008) in a modern Soreq Cave stalagmite as revealed by high-resolution geochemical analysis. Chem. Geol. 363, 322–333. https://doi.org/10.1016/j.chemgeo.2013.11.011.
Paterson, D., de Jonge, M.D., Howard, D.L., Lewis, W., McKinlay, J., Starritt, A., Kusel, M., Ryan, C.G., Kirkham, R., Moorhead, G., Siddons, D.P., McNulty, I., Eyberger, C., Lai, B., 2011. The X-Ray Fluorescence Microscopy Beamline at the Australian Synchrotron, pp. 219–222. https://doi.org/10.1063/1.3625343.
Richards, D.A., Bottrell, S.H., Cliff, R.A., Ströhle, K., Rowe, P.J., 1998. U-Pb dating of a speleothem of Quaternary age. Geochem. Cosmochim. Acta 62 (23), 3683–3688. https://doi.org/10.1016/S0016-7037(98)00256-7.
Ryan, C.G., Kirkham, R., Siddons, D.P., Dunn, P.A., Laird, J.S., Kuczewski, A., Moorhead, G., De Geronimo, G., Davey, P., Jensen, M., Paterson, D.J., de Jonge, M.D., Howard, D.L., Hough, R.M., 2010. The Maia 384 detector array in a nuclear microprobe: a platform for high definition PIXE elemental imaging. Nucl. Instrum. Methods Phys. Res. Sect. B Beam Interact. Mater. Atoms 268 (11), 1899–1902. https://doi.org/10.1016/j.nimb.2010.02.052.
Scholz, D., Hoffmann, D., 2008. 230Th/U-dating of fossil corals and speleothems. E&G – Quaternary Science Journal 57, 1–2. https://doi.org/10.23689/fidgeo-1056.
Scroxton, N., Walczak, M., Markowska, M., Zhao, J.-x., Fallon, S., 2021. Historical droughts in southeast Australia recorded in a new South wales stalagmite. Holocene 31 (4), 607–617. https://doi.org/10.1177/0959683620981717.
Stoddart, D.R., Woodroffe, C., Spencer, T., 1990. Mauke, Mitiaro and Atiu: Geomorphology of Makatea Islands in the Southern Cooks.
Stuiver, M., Polach, H.A., 1977. Discussion reporting of 14C data. Radiocarbon 19 (3), 355–363. https://doi.org/10.1017/S0033822200003672.
Sundqvist, H.S., Holmgren, K., Fohlmeister, J., Zhang, Q., Matthews, M.B., Spötl, C., Körnich, H., 2013. Evidence of a large cooling between 1690 and 1740 AD in southern Africa. Sci. Rep. 3 (1), 1767. https://doi.org/10.1038/srep01767.
Tan, M., Baker, A., Genty, D., Smith, C., Esper, J., Cai, B., 2006. Applications of stalagmite laminae to paleoclimate reconstructions: comparison with dendrochronology/climatology. Quat. Sci. Rev. 25 (17), 2103–2117. https://doi.org/10.1016/j.quascirev.2006.01.034.
Treble, P., Shelley, J.M.G., Chappell, J., 2003. Comparison of high resolution sub-annual records of trace elements in a modern (1911–1992) speleothem with instrumental climate data from southwest Australia. Earth Planet Sci. Lett. 216 (1), 141–153. https://doi.org/10.1016/s0012-821x(03)00504-1.
Treble, P.C., Chappell, J., Gagan, M.K., McKeegan, K.D., Harrison, T.M., 2005. In situ measurement of seasonal δ18O variations and analysis of isotopic trends in a modern speleothem from southwest Australia. Earth Planet Sci. Lett. 233 (1), 17–32. https://doi.org/10.1016/j.epsl.2005.02.013.
Trotter, M.M., Duff, R., 1974. Prehistory of the Southern Cook Islands. Canterbury Museum Trust Board.
Vansteenberge, S., de Winter, N.J., Sinnesael, M., Verheyden, S., Goderis, S., Van Malderen, S.J.M., Vanhaecke, F., Claeys, P., 2020. Reconstructing seasonality through stable-isotope and trace-element analyses of the Proserpine stalagmite, Han-sur-Lesse cave, Belgium: indications for climate-driven changes during the last 400 years. Clim. Past 16 (1), 141–160. https://doi.org/10.5194/cp-16-141-2020.
Wang, J.K., Johnson, K.R., Borsato, A., Amaya, D.J., Griffiths, M.L., Henderson, G.M., Frisia, S., Mason, A., 2019. Hydroclimatic variability in Southeast Asia over the past two millennia. Earth Planet Sci. Lett. 525, 115737 https://doi.org/10.1016/j.epsl.2019.115737.
Weir, T., Kumar, R., Ngari, A., 2021. Interdecadal modulation of the effect of ENSO on rainfall in the southwestern Pacific. Journal of Southern Hemisphere Earth Systems Science 71 (1), 53–65. https://doi.org/10.1071/ES19053.
Widlansky, M.J., Timmermann, A., Stein, K., McGregor, S., Schneider, N., England, M.H., Lengaigne, M., Cai, W., 2012. Changes in South Pacific rainfall bands in a warming climate. Nat. Clim. Change 3, 417. https://doi.org/10.1038/nclimate1726.
Xie, S.-P., Deser, C., Vecchi, G.A., Ma, J., Teng, H., Wittenberg, A.T., 2010. Global warming pattern formation: sea surface temperature and rainfall. J. Clim. 23 (4), 966–986. https://doi.org/10.1175/2009jcli3329.1.
Zhao, J.-x., Wang, Y.-j., Collerson, K.D., Gagan, M.K., 2003. Speleothem U-series dating of semi-synchronous climate oscillations during the last deglaciation. Earth Planet Sci. Lett. 216 (1), 155–161. https://doi.org/10.1016/S0012-821X(03)00501-6.